RSC Advances

PAPER

View Article Online
View Journal | View Issue

Cite this: *RSC Adv.*, 2020, **10**, 14208

Pt/Al_2O_3 coated with N-doped carbon as a highly selective and stable catalyst for catalytic hydrogenation of *p*-chloronitrobenzene to *p*-chloroaniline†

Donghong Zhu, Xin Weng, Yuqiong Tang, Jingya Sun, * Shourong Zheng and Zhaoyi Xu

Selective catalytic hydrogenation of *p*-chloronitrobenzene on Pt-based catalysts is a green and high-efficient way for *p*-chloroaniline production. However, supported monometallic Pt catalysts often exhibit undesirable *p*-chloroaniline selectivity. We herein reported supported Pt catalysts with N-doped carbon (NC) as an overcoating (Pt/Al_2O_3@NC) to overcome the disadvantage. Three Pt/Al_2O_3@NC catalysts with different NC coating amounts were prepared by *in situ* carbonization of an ionic liquid. For comparison, Al_2O_3 coated by NC and Pt/Al_2O_3 coated by SiO_2 were also prepared. A combination characterization confirmed that the NC overcoating was successfully formed on Pt/Al_2O_3 surface and Pt particles were completely coated by NC layers when ion liquid amount increased to 25 μl per g catalyst. Due to the intimate contact of NC layers and Pt particles Pt-NC heterojunctions were effectively formed on the catalyst surface. For the catalytic hydrogenation of *p*-chloronitrobenzene, Pt/Al_2O_3@NC with 25 μl ionic liquid as the NC precursor exhibited 100% selectivity to *p*-chloroaniline at 100% conversion of *p*-chloronitrobenzene. A lower ionic liquid amount led to decreased selectivity to *p*-chloroaniline. Furthermore, no deactivation was observed on Pt/Al_2O_3@NC during 5 catalytic cycles. The findings in the study demonstrate that coating noble metal catalysts by N-doped carbon is a promising method to enhance the selectivity and stability for catalytic hydrogenation of *p*-chloronitrobenzene.

Received 19th February 2020
Accepted 12th March 2020

DOI: 10.1039/d0ra01578d

rsc.li/rsc-advances

1. Introduction

As important chemical raw materials, chloroanilines (CANs) are widely used as intermediates in pharmaceuticals, herbicides, pigments and dyes.[1–3] Conventionally, CANs could be produced *via* reduction of corresponding chloronitrobenzenes (CNBs) using stoichiometric reductants such as potassium borohydride and hydrazine hydrate.[2–4] However, the use of stoichiometric reductants would bring large amounts of harmful waste and severe pollution to the environment. Alternatively, selective catalytic hydrogenation reduction is an eco-friendly and cost-effective method for the conversion of CNBs to CANs.

For catalytic hydrogenation reduction, noble metals such as Pd and Pt are highly active because of their strong abilities for H_2 activation under mild conditions.[5,6] However, supported noble metal catalysts exhibited low selectivity because dechlorinated byproducts were inevitably formed due to their strong hydrodechlorination capabilities.[5,7] For example, supported Pt catalysts were considered as the most selective ones among supported noble metals for the catalytic conversion of CNBs to CANs,[3,8,9] however, Pt/C catalyst only displayed 75.2% selectivity to *p*-CAN at 100% conversion of *p*-CNB.[10] Additionally, catalyst deactivation often occurs as a result of contamination of metal surface or/and metal leaching during the reaction processes.[11,12] For example, Mahata *et al.*[11] found that Pt/CNT deactivated drastically in the catalytic hydrogenation of *o*-CNB during the second and subsequent reaction runs. Hence, exploring effective strategies to improve the catalytic selectivity and stability of supported noble metal catalysts for hydrogenation of CNBs to corresponding CANs is of significant importance.

Many attempts such as addition of a promoting metal or decorating metal particles with organic modifiers have been made to improve the catalytic selectivity for *p*-CNB hydrogenation.[13–17] For example, Zhu *et al.*[18] prepared a core–shell structural bimetallic Pt@Cu/TiO_2 catalyst with monolayer Cu as the shell for catalytic hydrogenation of *p*-CNB and obtained 100% selectivity to *p*-CAN. Very recently, coating supported catalysts have been proved to be an effective approach to enhance catalytic selectivity. Chen *et al.*[14] prepared a Pt-nanowire catalyst chelated by ethylenediamine on catalyst surface, which exhibited prominent selectivity for the catalytic production of *N*-

State Key Laboratory of Pollution Control and Resource Reuse, School of the Environment, Nanjing University, Nanjing 210046, China. E-mail: sunsun1118@126.com; Fax: +86-25-89680596; Tel: +86-25-89680373

† Electronic supplementary information (ESI) available. See DOI: 10.1039/d0ra01578d

hydroxylanilines from nitrobenzene. Leng *et al.*[19] reported that controlled and chemoselective hydrogenation of nitrobenzene was achieved on a $Ru@C_{60}$ catalyst. Notably, coating supported catalysts was also reported as a prominent strategy to enhance catalytic stability through protecting metal particles from leaching and poisoning. For example, Fu *et al.*[20] illustrated that a Ni/Al_2O_3 catalyst coated with carbon nitride layer provided an exceptional stability for the catalytic hydrogenation of nitrobenzene. Li *et al.*[21] developed a Pt catalyst with Pt particles embedded in N-doped carbon rods and observed a superior catalytic stability in the liquid-phase catalytic hydrogenation of bromate. Recent years, N-doped carbon (NC) materials have attracted tremendous attentions because of their unique and versatile properties. For example, N-doped carbon could transfer electrons to metal particles or *vice versa via* metal–NC heterojunctions and thus serve as catalytically active sites for the adsorption and activation of H_2 and reactants.[20–22] Inspired by recent advances, it is reasonable to speculate that coating supported noble metal catalysts with N-doped carbon may probably improve the catalytic selectivity and stability for hydrogenation of CNBs. However, few studies have been conducted for the selective hydrogenation of *p*-CNB on coated noble metal catalysts thus far.

The main objective of the present study is to develop highly selective and stable supported Pt catalysts for the catalytic hydrogenation of CNBs to CANs. We prepared three Pt/Al_2O_3 catalysts coated by NC layer with different NC amounts by *in situ* carbonization of ion liquid (1-ethyl-3-methylimidazolium dicyanamide, EMIm-dca). For comparison, Al_2O_3 coated with NC and Pt/Al_2O_3 coated with SiO_2 were also prepared. The structural properties of the synthesized catalysts were characterized by a series of techniques and the catalytic performances of the catalysts for hydrogenation of *p*-CNB were examined.

2. Experimental

2.1 Catalyst preparation

Chemical and materials. Ion liquid (EMIm-dca) and hydrogen hexachloroplatinate(IV) hexahydrate ($H_2PtCl_6 \cdot 6H_2O$) were purchased from Aldrich. Aluminum isopropoxide, oleylamine, sodium silicate, ammonium hydroxide ($NH_3 \cdot H_2O$), hydrogenchloride (HCl), nitric acid (HNO_3), *p*-CNB, and *p*-CAN were obtained from Sinopharm Chemical Reagent Co., Ltd., China. All chemicals were used without further purification.

Preparation of aluminum sol. A desired amount of aluminum isopropoxide powder was added slowly into 150 ml distilled water with a molar ratio of water to aluminum isopropoxide of 100 : 1 in a three-necked round flask under vigorous stirring at 80 °C for controlled hydrolysis of aluminum isopropoxide. After refluxing at 80 °C for 1 h, the mixture was further evaporated at 90 °C for 1 h to remove formed alcohol. The pH of the mixture was then adjusted to 3.0 using 10% HNO_3 solution. Aluminum sol was obtained after the mixture further refluxed at 80 °C for 24 h.

Preparation of Al_2O_3. Al_2O_3 was prepared using method reported by Fu *et al.*[20] Briefly, 180 g of alumina sol, 14 g of oleylamine and 10 ml of 25% $NH_3 \cdot H_2O$ was dispersed in 150 ml of distilled water at 80 °C in a water bath. After stirring for 2 h at 80 °C, the mixture was transferred into the autoclave, sealed and kept at 180 °C for 72 h in an oven. The resulting mixture was filtered and washed using ethanol for several times and then oven-dried at 100 °C. Finally, the obtained powder was calcined at 550 °C in a muffle furnace for 4 h.

Preparation of Pt/Al_2O_3. Pt/Al_2O_3 was prepared using a conventional impregnation method with H_2PtCl_6 as metal precursor. Briefly, 1 g of grinded and sieved Al_2O_3 was impregnated with 2.7 ml of 1.9×10^{-5} mol ml^{-1} H_2PtCl_6 solution. After stirring for 2 h, the mixture was evaporated under 80 °C in a water bath. The sample was oven-dried at 100 °C overnight and calcined in a muffle furnace at 300 °C for 4 h. The nominal content of Pt was 1 wt%.

Preparation of Pt/Al_2O_3@NC. Pt/Al_2O_3@NC was prepared by a reported method with ion liquid (EMIm-dca) as NC precursor.[23] Briefly, 1 g Pt/Al_2O_3 and a desired amount of ion liquid (10, 15 and 25 μl of EMIm-dca, respectively) were added in a 20 ml of beaker containing 5 ml of distilled water. After mixed well by ultrasonic treatment, the slurry was dried at 70 °C in a porcelain boat and calcined in a tubular furnace with a heating rate of 5 °C min^{-1} up to 400 °C and maintained at this temperature for 1 h under N_2 atmosphere. For comparison, Al_2O_3@NC without Pt loading was also prepared. The resulting catalysts were labeled as Pt/Al_2O_3@NC-*X* or Al_2O_3@NC-*X*, where *X* refers to the amount of ion liquid added. The prepared Pt/Al_2O_3@NC-25 was further calcined at 500 °C in air for 2 h to remove the NC overcoating to clarify the role of NC. This catalyst was labelled as Pt/Al_2O_3@NC-25-calcined. All the catalysts were pre-reduced in H_2 atmosphere at 300 °C for 2 h in prior to the characterization and evaluation of catalytic activity.

Preparation of $Pt/Al_2O_3@SiO_2$. $Pt/Al_2O_3@SiO_2$ was prepared using method reported by Li *et al.*[12] Briefly, 1 g of Pt/Al_2O_3 was dispersed in 200 ml of distilled water, which was stabilized at 80 °C under a 30 ml min^{-1} N_2 flow. Under vigorous stirring, 20 ml of sodium silicate solution (1.0 mol l^{-1}) was added to the suspension dropwise, and then the pH of the mixture was adjusted to 6.0 using a HCl solution (1 mol l^{-1}). The mixture was further stirred at 80 °C for 30 h. The catalyst was obtained after washed with distilled water for several times and dried at 65 °C under vacuum for 10 h.

2.2 Catalyst characterization

Pt contents in the samples were precisely determined by an inductively coupled plasma-atomic emission spectrometer (ICP-AES) (J-A1100, Jarrell-Ash, USA). The XRD patterns of the samples were collected on a Rigaku D/max-RA powder diffraction-meter using a Cu Kα radiation (Rigaku, Tokyo, Japan). The carbon and nitrogen contents in the catalysts were determined using an elementary analyzer CHN–O-rapid apparatus (Heraeus, Germany). The Brunauer–Emmett–Teller (BET) surface areas of the catalysts were measured using a Micromeritics ASAP 2200 instrument (Micromeritics Instrument Co., Norcross, GA). High-angle annular dark field-scanning transmission electron microscope (HAADF-STEM) and elemental mapping images were acquired using an ARM-200F

transmission electron microscope (JEOL Co., Japan.) equipped with an X-MAX energy dispersive spectrometer (Oxford, UK). X-ray photoelectron spectroscopy (XPS) spectra were recorded on a PHI5000 VersaProbe with a monochromatized Al Kα X-ray source ($h\nu$ = 1486.6 eV) (ULVAC-PHI, Japan). The binding energy was calibrated by measuring the C 1s peak at 284.6 eV.

Temperature programmed oxidation (TPO) was conducted on an AMI-300 setup (Altamira Instruments, USA) with a gas analysis system (Thermo Star, Germany). Typically, 50 mg of catalyst was loaded in a U-shaped quartz tube, which was pre-treated at 120 °C for 1 h using a 25 ml min^{-1} of He flow in a heating furnace. After cooling down, the catalyst was *in situ* oxidized with a 5% O_2/He flow (25 ml min^{-1}) from ambient temperature to 600 °C at a rate of 5 °C min^{-1}. The evolved gases were monitored with intensities of m/z 17 (NH_3), 28 (CO), 30 (NO), 44 (CO_2) and 46 (NO_2), respectively.

2.3 Catalytic hydrogenation of *p*-chloronitrobenzene

The catalytic hydrogenation of *p*-CNB over the catalysts was conducted in a high pressure stainless steel autoclave with a controlling system. Briefly, 20 mg catalyst, 100 mg *p*-CNB and 20 ml ethanol was added to the autoclave. Before hydrogenation reaction, the autoclave was flushed with N_2 for 5 times to replace air in the reactor under ambient condition. The reaction was conducted under 1 MPa pressure of H_2 at 80 °C with stirring rate fixing at 1000 rpm. Samples were taken periodically and detected by a 6980 gas chromatograph equipped with a FID detector and a DB-5 capillary column (Agilent Technologies, US), and *n*-hexane was used as the inner standard substance. For catalyst reuse, the used catalyst was prepared under the same reaction conditions but without sampling. After reaction for 180 min, the catalyst was collected by filtration, rinsing with ethanol and distilled water and drying at 60 °C for 12 h. The catalyst was then subjected to the subsequent reaction test.

The conversion of *p*-CNB and selectivity to *p*-CAN and aniline were calculated following equations below:

$$\text{Conversion} = \frac{m_{(p\text{-CNB})0} - m_{(p\text{-CNB})t}}{m_{(p\text{-CNB})0}} \times 100\% \quad (1)$$

$$\text{Selectivity}_{(p\text{-CAN})} = \frac{m_{(p\text{-CAN})t}}{m_{(p\text{-CAN})t} + m_{(\text{aniline})t}} \times 100\% \quad (2)$$

$$\text{Selectivity}_{(\text{aniline})} = \frac{m_{(\text{aniline})t}}{m_{(p\text{-CAN})t} + m_{(\text{aniline})t}} \times 100\% \quad (3)$$

where m refers to the molar amount.

3. Results and discussion

3.1 Catalyst characterization

Table 1 shows Pt content of the catalysts determined by ICP-AES. For Pt/Al_2O_3, Pt content was determined to be 0.96 wt%. As for Pt/Al_2O_3@NC, Pt content were in the range of 0.71–0.78 wt%, which were lower than that of Pt/Al_2O_3 due to successful loading of NC overcoating.

The compositions of C and N elements in the catalysts were determined by elemental analysis and the results are

Table 1 Structural properties of the catalysts

Catalysts	Pt content[a] (wt%)	C content[b] (wt%)	N content[b] (wt%)	Surface concentration of N[c] (at%)	N_1/N_2[c]	BET surface area[d] ($m^2\ g^{-1}$)	d_1[e] (nm)	CO adsorption amount[f] (μmol g^{-1})	Coverage of Pt surface[f] (%)	d_2[f] (nm)
Pt/Al_2O_3	0.96	BDL	BDL	BDL	BDL	103	4.0	12.0	—	4.3
Pt/Al_2O_3@NC-10	0.78	0.33	0.17	0.49	BDL	100	3.9	3.7	69%	—
Pt/Al_2O_3@NC-15	0.71	0.63	0.30	0.65	0.92	101	4.0	0.5	96%	—
Pt/Al_2O_3@NC-25	0.78	0.76	0.39	0.79	0.71	99	4.1	0	100%	—
Al_2O_3@NC-25	BDL[g]	0.58	0.24	0.61	0.47	110	—	BDL	—	—

[a] Determined by ICP. [b] Determined by elemental analysis. [c] Determined by XPS, N_1/N_2 refers to the ratio of pyridinic N amount to pyrrole N amount on catalyst surface. [d] Calculated from BET. [e] Calculated from HAADF-STEM. [f] Calculated by CO chemisorption. [g] Below determine limit.

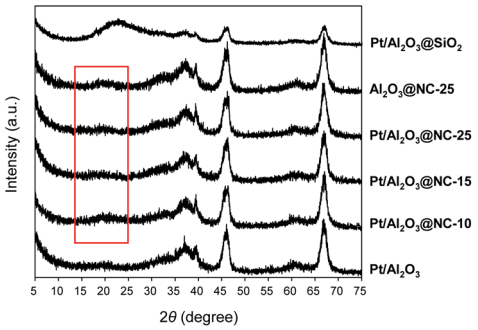

Fig. 1 XRD patterns of the catalysts.

summarized in Table 1. For Pt/Al_2O_3@NC-10, Pt/Al_2O_3@NC-15 and Pt/Al_2O_3@NC-25, the C contents were 0.33%, 0.63% and 0.76% respectively, exhibiting increased C content with the increase of ion liquid loading amount from 10 μl to 25 μl. Consistently, N contents in Pt/Al_2O_3@NC catalysts increased from 0.17% to 0.39% with ion liquid loading. For Al_2O_3@NC-25, the C and N content were determined to be 0.58% and 0.24% respectively, lower than those of Pt/Al_2O_3@NC-25, probably because the presence of Pt particles on Al_2O_3 surface stabilized the NC matrix formed by pyrolysis of ion liquid *via* evoking interactions with NC matrix. The molar N/C ratios in the catalysts were in the range of 0.35–0.44 which was lower than 0.63 of ion liquid, this can be ascribed to more prominent loss of unstable N species upon carbonization at high temperatures.[24,25]

Fig. 1 shows the XRD patterns of the catalysts in the range of 20–80°. Diffraction peaks centered at 37.3°, 39.5°, 45.7°, and 67.1° indexed to the γ-Al_2O_3 phase, were clearly observed on all the catalysts. No diffraction peaks characteristic of Pt were found in the XRD patterns probably due to low metal contents of the catalysts.[26] Notably, in the range of 15–25°, a weak and broad peak centered at 19.5° were observed on Pt/Al_2O_3@NC catalysts. The very weak peak was ascribed to amorphous N-doped carbon, which was lower than that of amorphous carbon (23.5°) due to the increase of inter-layer distance of carbon upon N doping.[27] As for the XRD pattern of Pt/Al_2O_3@-SiO_2, the broad peak centered at 23.1° was assigned to amorphous silica. In comparison with Pt/Al_2O_3@NC, Pt/Al_2O_3@SiO_2 had markedly weakened intensities of peaks of γ-Al_2O_3 phase, likely resulting from the thicker SiO_2 overcoating than NC overcoating.

Fig. S1, ESI† shows the HAADF-STEM images of the catalysts. Al_2O_3 had uniform rhombus morphology with diameter in the range of 30–60 nm. The TEM images showed that Pt particles were spherical and were well dispersed on Al_2O_3 surface. The average Pt particle diameter was measured based on the surface area weighted diameter:[28,29]

$$\overline{d_s} = \sum n_i d_i^3 \Big/ \sum n_i d_i^2 \quad (4)$$

where n_i is the number of selected Pt particles having diameter of d_i and the selected total particle number ($\sum n_i$) exceeds 100.

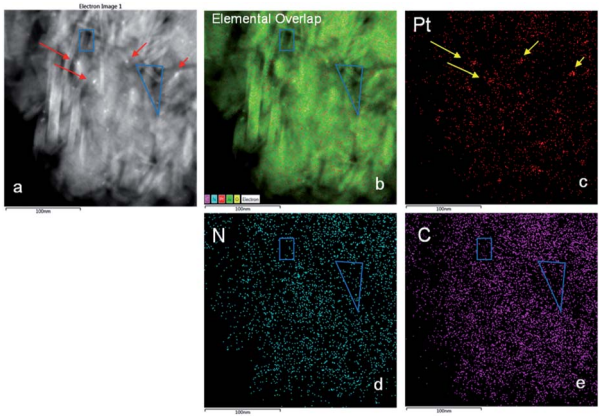

Fig. 2 (a) HAADF-STEM image of Pt/Al_2O_3@NC-25 and the corresponding EDS elemental mapping of (b) the overlapping of Pt, C, and N element, (c) Pt element (red), (d) N element (blue), and (e) C element (purple).

Results are listed in Table 1. The average sizes of Pt particles of Pt/Al_2O_3, Pt/Al_2O_3@NC-10, Pt/Al_2O_3@NC-15 and Pt/Al_2O_3@NC-25 were 4.0, 3.9, 4.0 and 4.1 nm, respectively, indicating that NC coating did not affect the structure of Pt/Al_2O_3. However, NC overcoating layer was not clearly visible in TEM images, probably because of the very low NC contents (as indicated by elemental analysis results). To verify the presence of NC overcoating on the catalysts, EDS mapping analysis was conducted on Pt/Al_2O_3@NC-25 and the images are presented in Fig. 2. In Fig. 2a light particles with diameter around 5–7 nm could be clearly observed as marked by red arrows. Consistently, Pt signal was very dense in the same area in the mapping image in Fig. 2c, reflecting that the lightness variation was due to the presence of Pt particles on Al_2O_3 support. The EDS mapping of elemental C and N in Pt/Al_2O_3@NC-25 (see Fig. 2d and e) showed that elemental C and N were evenly distributed on Al_2O_3 surface. The clear spatial correlation among elemental Al, C and N was indicative of a close contact of NC with Al_2O_3 support, verifying the presence of NC overcoating on Al_2O_3 surface.

To further investigate the composition of Pt/Al_2O_3@NC-25, temperature-programed oxidation of Pt/Al_2O_3@NC-25 was

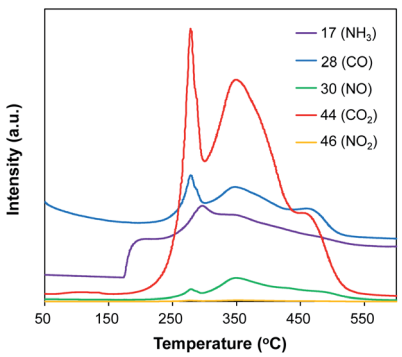

Fig. 3 Temperature programmed oxidation profile of Pt/Al_2O_3@NC-25.

conducted, and the dependence of gas release on oxidation temperature are shown in Fig. 3. In Fig. 3, CO and CO_2 exhibited very similar evolving profiles, in which a strong and broad peak with two shoulders presented in the range of 200–550 °C. In parallel, marked release of NH_3 and NO was also observed in the range of 180–530 °C. The presence of CO_2, CO, NH_3 and NO_2 could be ascribed to the oxidation of C and N containing species, confirming the presence of NC overcoating on the catalyst surface.[30] Notably, the oxidation temperature of N species was slightly lower than that of C species, reflecting that N species were more prone to lose than C species upon high temperature, in line with elemental analysis results.

The effective decoration of NC overcoating on Pt particle could be further verified by CO chemisorption (see Table 1). The CO adsorption amount on Pt/Al_2O_3 was determined to be 12.0 μmol g^{-1}. Accordingly, the average diameter of Pt particles of Pt/Al_2O_3 could be calculated by CO chemisorption amount with a chemisorption stoichiometry of CO/Pt = 1. The diameter was calculated to be 4.3 nm, in good agreement with that measured by TEM. After NC coating, the CO adsorption amount markedly decreased. For example, CO adsorption amount of Pt/Al_2O_3@NC-10 and Pt/Al_2O_3@NC-15 was 3.7 μmol g^{-1} and 0.5 μmol g^{-1} respectively, much lower than that of Pt/Al_2O_3. Because CO could chemically adsorb only on exposed Pt sites of the catalyst, the decreased chemisorption amount of CO clearly reflected lowered exposure of Pt sites of the catalysts as a result of NC overcoating.[31] Further increasing NC coating amount even led to the absence of CO adsorption on Pt/Al_2O_3@NC-25, indicating that Pt sites were completely blocked by NC overcoating in the catalyst. For Pt/Al_2O_3@NC-25 calcined at 500 °C in air, the CO chemisorption amount increased to 7.0 μmol g^{-1} (see Table 3). Because calcination led to the oxidation of NC matrix of the catalyst and thus resulted in the exposure of blocked Pt sites for CO chemisorption. Notably, the CO chemisorption amount of Pt/Al_2O_3@NC-25-calcined was lower than that of Pt/Al_2O_3, probably due to incomplete oxidation of NC overcoating upon calcination.

Fig. 4 shows the XPS spectra of the catalysts. Because Pt 4f region was overlapped by the strong Al 3p peak, the surface Pt compositions of the catalysts were analyzed by XPS spectra in Pt 4d region. In Fig. 4a, two peaks around 315.2 and 332.7 eV were found for Pt/Al_2O_3, characteristic of Pt $4d_{5/2}$ and $4d_{3/2}$, respectively (see Fig. 4a).[32,33] Upon NC coating, slightly lowered binding energies of Pt 4d were observed. For example, the binding energies of Pt $4d_{5/2}$ was 315.0, 314.8 and 314.7 eV for Pt/Al_2O_3@NC-10, Pt/Al_2O_3@NC-15 and Pt/Al_2O_3@NC-25 respectively. The gradual red shift of the binding energy of Pt $4d_{5/2}$ with NC coating amount in the catalysts may be ascribed to the electron transfer from electronic-enriched N sites to Pt due to their strong interactions.[34,35] Fig. 4b shows XPS spectra of the catalysts in the N 1s region. Deconvolution of the N 1s peak gave rise to two peaks located at 398.6 and 400.2 eV, characteristic of pyridinic N and pyrrole N respectively, further confirming the successful formation of NC overcoating layers. The ratio of pyridinic N to pyrrole N of the catalysts were calculated and the results are summarized in Table 1. Notably, the ratio of pyridinic N (N_1) to pyrrole N (N_2) markedly differed with samples. For Al_2O_3@NC-25, the ratio of N_1/N_2 was 0.47, which was much lower than that of Pt/Al_2O_3@NC-25 (0.71). In comparison with Pt/Al_2O_3@NC-25, Pt/Al_2O_3@NC-15 with

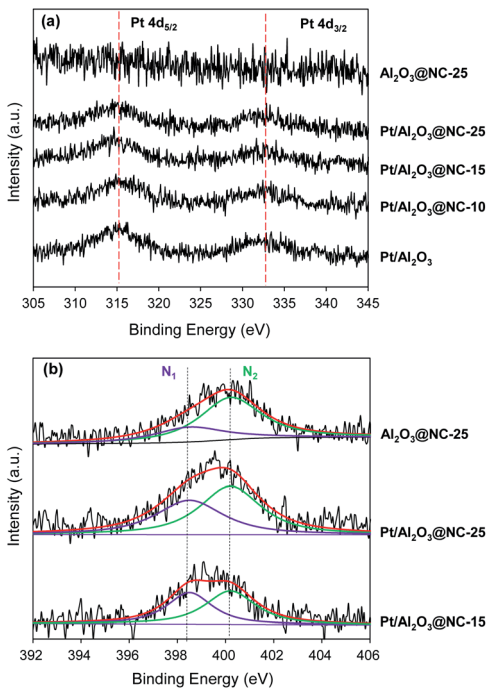

Fig. 4 XPS spectra of catalysts in the regions of (a) Pt 4d and (b) N 1s.

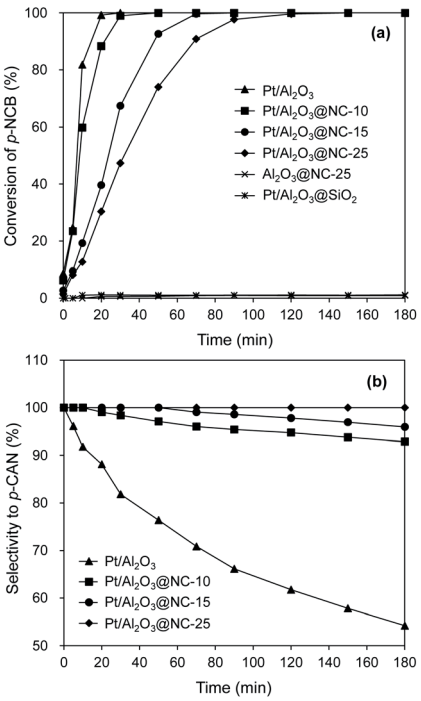

Fig. 5 Catalytic hydrogenation of *p*-CNB on the catalysts. Reaction conditions: catalyst dosage: 20 mg, alcohol: 20 ml, *p*-NCB amount: 100 mg, reaction temperature: 80 °C, H_2 pressure: 1 MPa.

a lower NC content has a higher N_1/N_2 ratio of 0.92. Notably, binding energy in N 1s region characteristic of covalently bound N–Pt species was found to be 398.6 eV, which was identical to the binding energy of pyridinic N.[36] Hence, the much higher N_1/N_2 ratio in Pt/Al_2O_3@NC-25 than that of Al_2O_3@NC-25 could be attributed to the formation of additional N–Pt species when ion liquid was pyrolyzed on catalyst surface. The results clearly confirmed strong interactions between Pt and N atoms in NC matrix as also indicated by elemental analysis results. Consistently, the higher N_1/N_2 ratio of Pt/Al_2O_3@NC-15 can be explained in terms of the formation of more Pt–N species as a result of the higher Pt : N ratio in Pt/Al_2O_3@NC-15 than that of Pt/Al_2O_3@NC-25 assuming identical Pt sites in Pt/Al_2O_3@NC-15 to those in Pt/Al_2O_3@NC-25.

3.2 Catalytic hydrogenation of *p*-CNB

The catalytic performances of the catalysts for hydrogenation of *p*-CNB are presented in Fig. 5 and the reaction constants are compared in Table 2. Aniline and *p*-CAN were identified as products in all the reactions. Control experiment showed that Al_2O_3@NC-25 exhibited very low activity for catalytic hydrogenation of *p*-CNB with *p*-CNB conversion of 0.6% within 180 min of reaction time, reflecting the very weak capability of NC overcoating and Al_2O_3 for H_2 activation under reaction conditions. In contrast, Pt/Al_2O_3 exhibited a much higher catalytic activity with 100% of *p*-CNB conversion within 30 min indicating the high activity of Pt particles for H_2 activation and *p*-CNB reduction. Upon NC coating, the conversion of *p*-CNB over Pt/Al_2O_3@NC gradually decreased with NC coating amount. For example, *p*-CNB was completely converted at 50, 90, and 150 min on Pt/Al_2O_3@NC-10, Pt/Al_2O_3@NC-15 and Pt/Al_2O_3@NC-25 respectively (see Table 2). The deteriorated catalytic activity of Pt/Al_2O_3@NC was likely due to blocking Pt sites by NC overcoating from *p*-CNB as evidenced by CO chemisorption results. Accordingly, decreased catalytic activity as a result of coating catalyst surface had been reported previously.[37,38] Notably, effective hydrogenation of *p*-CNB was found on Pt/Al_2O_3@NC-25 although Pt sites were completely blocked by NC matrix (see CO chemisorption results). This results suggested that H_2 was capable of being activated and *p*-CNB could be reduced on NC matrix on catalyst surface. Considering the negligible catalytic activity of Al_2O_3@NC-25, a synergistic effect between Pt and NC overcoating could be deduced. Previous reports proved that supported metal catalysts with carbonaceous materials as the overcoating could catalyze hydrogenation reactions.[20,21,37] It was proposed that intimate contact between metal and carbon matrix would cause a metal–carbon matrix heterojunction, through which H_2 could be adsorbed and activated and electrons could be transferred to reactants. Accordingly, the mechanism well explained the hydrogenation of *p*-CNB on Pt/Al_2O_3@NC-25. XPS results confirmed strong interactions between Pt particles and NC matrix, forming Pt-NC heterojunction. Furthermore, the catalytic performance of the catalyst with non-conductive overcoating also confirmed this mechanism. For example, Pt/Al_2O_3 coated by SiO_2 exhibited negligible catalytic activity for hydrogenation of *p*-CNB (1.1% *p*-CNB conversion in 180 min reaction time) (see Table 2). This was because that SiO_2 is an inert insulator, on which electron transfer was substantially suppressed, thus resulting in a negligible catalytic activity than that of Pt/Al_2O_3@NC-25. Similarly, Li *et al.*[12] observed a much higher catalytic activity of Pd/CNT with N-doped carbon as overcoating than that of SiO_2 coated Pd/CNT for catalytic reduction of Cr (VI) in liquid phase.

Besides catalytic activity coating Pt/Al_2O_3 substantially impacted the selectivity in catalytic hydrogenation of the *p*-CNB. For example, Pt/Al_2O_3 displayed a catalytic selectivity of 81.8% to *p*-CAN at 100% of *p*-CNB conversion, suggesting that Pt sites were active for both reduction of NO_2 group and activation of C–Cl bond in *p*-CNB. In contrast, Pt/Al_2O_3@NC exhibited significantly improved *p*-CAN selectivity, and the selectivity to *p*-CAN was strongly dependent on NC overcoating amount. Specifically, increasing ion liquid amount to 25 μl per g catalyst resulted in *p*-CAN selectivity increasing monotonically from 81.8% to 100% at 100% conversion of *p*-CNB, indicating effective inhibition of hydrodechlorination owing to NC coated on the surface of Pt particles. Notably, because Cl group in *p*-CNB would increase the electron density of NO_2 group, the reduction of NO_2 group in *p*-CNB was favored by the presence of Cl group.[3,39] Accordingly, *p*-CAN is the main production in the hydrogenation of *p*-CNB. After *p*-CNB was 100% converted, however, the catalytic selectivity to *p*-CAN markedly decreased on all catalysts except Pt/Al_2O_3@NC-25. For example, the selectivity to *p*-CAN on Pt/Al_2O_3, Pt/Al_2O_3@NC-10 and Pt/Al_2O_3@NC-15 decreased to 54.2%, 92.8% and 95.9% after 180 min of reaction time, respectively. In contrast, Pt/Al_2O_3@NC-25 maintained 100% selectivity to *p*-CAN throughout the catalytic hydrogenation process even when only *p*-CAN left in the reaction system, clearly indicating that the catalytic dechlorination of *p*-CAN was completely inhibited on Pt/Al_2O_3@NC-25. In parallel, CO chemisorption showed that the coverage of Pt surface were 69%, 96% and 100% for Pt/Al_2O_3@NC-10, Pt/Al_2O_3@NC-15 and Pt/Al_2O_3@NC-25 respectively (see Table 1), confirming that C–Cl bond could only be cleaved on exposed Pt sites and NC overcoating was incapable of catalytic hydrodechlorination. Accordingly, the catalytic hydrogenation of *p*-CNB on Pt/Al_2O_3 and Pt/Al_2O_3@NC-25 were depicted in Scheme 1.

Table 2 Catalytic performances of the catalysts[a]

Catalysts	Reaction time (min)	Conversion (%)	*p*-CAN selectivity (%)	Aniline selectivity (%)
Pt/Al_2O_3	30	100.0	81.8	18.2
Pt/Al_2O_3@NC-10	50	100.0	97.1	2.9
Pt/Al_2O_3@NC-15	90	100.0	98.6	1.4
Pt/Al_2O_3@NC-25	150	100.0	100.0	0.0
Al_2O_3@NC-25	180	0.6	100.0	0.0
Pt/Al_2O_3@SiO_2	180	1.1	100.0	0.0

[a] Reaction conditions: catalyst dosage: 20 mg, alcohol: 20 ml, *p*-nitrochlorobenzene: 100 mg, reaction temperature: 80 °C, reaction time: 60 min; H_2 pressure: 1 MPa.

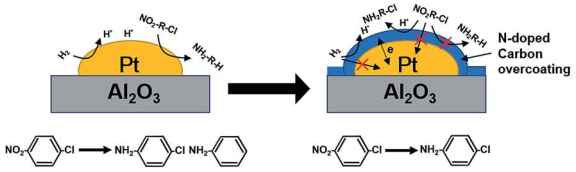

Scheme 1 Schematic illustration of catalytic hydrogenation of *p*-CNB on Pt/Al_2O_3 and Pt/Al_2O_3@NC-25.

To further explore the effect of NC overcoating on the catalytic performances of the coated catalysts. Pt/Al_2O_3@NC-25 was calcined at 500 °C in air for 2 h to remove NC coating and the catalytic hydrogenation of *p*-CNB was conducted on the calcined catalyst. The results are presented in Fig. 6. In comparison with Pt/Al_2O_3@NC-25, Pt/Al_2O_3@NC-25-calcined exhibited a significantly enhanced catalytic activity, which was very close to that of Pt/Al_2O_3. The increased catalytic activity of Pt/Al_2O_3@NC-25-calcined can be explained by the removal of NC overcoating on catalyst surface *via* calcination as reflected by TPO and CO chemisorption results. However, the catalytic selectivity of Pt/Al_2O_3@NC-25-calcined was still much higher than that of Pt/Al_2O_3, with a slightly decreased selectivity of 97.9% after 180 min reaction time in comparison with Pt/Al_2O_3@NC-25. CO chemisorption suggested that partial NC matrix remained on Pt/Al_2O_3@NC-25-calcined surface. Hence, the high selectivity of Pt/Al_2O_3@NC-25-calcined was probably related with NC matrix left on catalyst surface. On one hand, the remaining NC matrix would block partial Pt sites from catalytic hydrodechlorination. On the other hand, the interactions between Pt sites and residual NC matrix impacted the catalytic selectivity of Pt/Al_2O_3@NC-25-calcined. XPS results suggested that strong interactions and electron transfer existed between NC overcoating and Pt, causing negatively charged Pt sites. Because NH_2 groups in *p*-CAN tended to donate electron to Cl groups, which would give rise to electrostatic repulsion between Cl group and negatively charged Pt sites and thus suppressed the cleavage of C–Cl bond.[10,40,41] Similarly, Shi *et al.*[35] reported that Pt supported on N-doped carbon nanotube exhibited high selectivities to haloanilines for catalytic hydrogenation of halonitrobenzenes because of the electron-rich chemical state of Pt particles.

The stability of catalyst is of important significance for supported noble metal catalysts. For stability test, the consecutive catalytic hydrogenation of *p*-CNB was examined on Pt/Al_2O_3@NC-25 and results are shown in Fig. 7. It was very interesting to find that in the initial two cycles markedly increased activity of Pt/Al_2O_3@NC-25 from 47.3% to 100% at 30 min reaction time was observed, likely due to the presence of exposed Pt sites as a result of partial elimination of NC overcoating *via* washing catalyst surface by reaction solution. Accordingly, previous studies indicated that surface coke of used catalysts could be partially removed *via* washing by organic solvents.[42] Consistently, characterization results showed that CO chemisorption amount of Pt/Al_2O_3@NC-25 was 4.3 μmol g^{-1} after 5 catalytic cycles (see Table 3), reflecting a portion of Pt sites were again exposed. After 5 catalytic cycles, the catalytic activities remained constant and no catalyst deactivation was observed indicative of a very high catalytic stability of Pt/Al_2O_3@NC-25. HAADF-STEM and ICP results showed that the

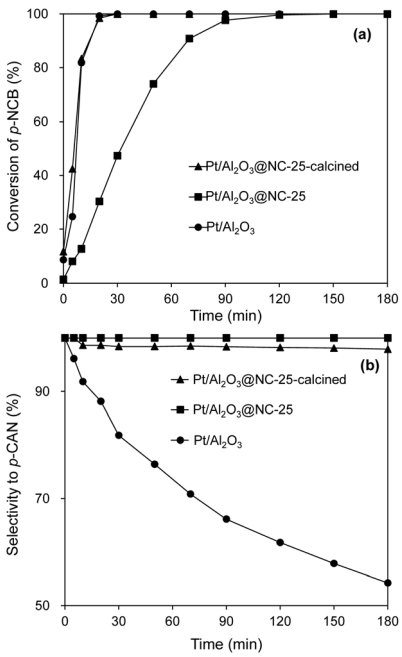

Fig. 6 Catalytic hydrogenation of *p*-CNB on Pt/Al_2O_3@NC-25-calcined in comparison with Pt/Al_2O_3@NC-25 and Pt/Al_2O_3. Reaction conditions: catalyst dosage: 20 mg, alcohol: 20 ml, *p*-NCB amount: 100 mg, reaction temperature: 80 °C, H_2 pressure: 1 MPa.

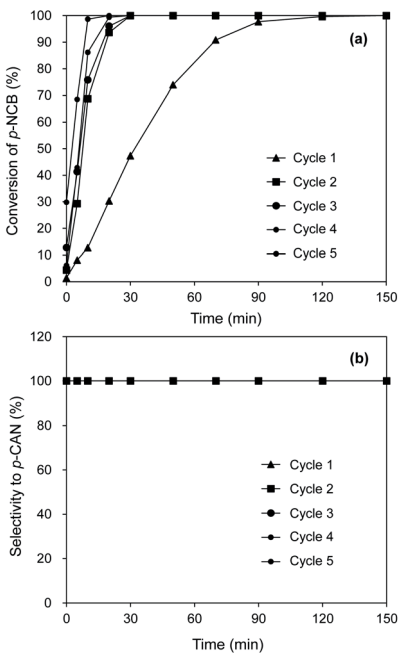

Fig. 7 The reuse of Pt/Al_2O_3@NC-25 for catalytic hydrogenation of *p*-CNB. Reaction conditions: catalyst dosage: 20 mg, alcohol: 20 ml, *p*-NCB amount: 100 mg, reaction temperature: 80 °C, H_2 pressure: 1 MPa.

Table 3 Structural properties of the catalysts

Catalysts	CO adsorption amount[a] (μmol g^{-1})	d^b (nm)	Pt content[c] (wt%)
Pt/Al_2O_3@NC-25-calcined	7.0	—	—
Pt/Al_2O_3@NC-25-cycled	4.3	3.8	0.77

[a] Calculated by CO chemisorption. [b] Calculated from HAADF-STEM results. [c] Determined by ICP.

particle size of Pt and Pt content of Pt/Al_2O_3@NC-25-cycled were very similar to those of the fresh Pt/Al_2O_3@NC-25, further confirming the high stability of Pt/Al_2O_3@NC-25 (see Table 3). Similarly, enhanced stability of supported metal catalyst *via* carbon coating was also reported previously.[43] Notably, although enhanced catalytic activity of Pt/Al_2O_3@NC-25 was observed and partial Pt sites were exposed on the catalyst surface after 2 reaction cycles, the catalytic selectivities to *p*-CAN were not accordingly decreased and remained 100% after 180 min reaction time in 5 reaction cycles, confirming that the electronic effect between Pt and NC overcoating played an important role in the high selectivity of the used Pt/Al_2O_3@NC-25.

4. Conclusions

In the present work, we prepared a series of Pt/Al_2O_3@NC catalysts with different ion liquid amount and investigated selective catalytic hydrogenation of *p*-CNB on the catalysts. Characterization results showed that NC matrix was formed as overcoating on Pt/Al_2O_3 surface, which blocked exposed Pt sites effectively. Furthermore, strong interactions existed between Pt sites and N atoms in NC matrix and their interactions led to electron-enrichment of Pt atoms. For the selective catalytic hydrogenation of *p*-CNB to *p*-CAN, Pt/Al_2O_3@NC-25 exhibited marked hydrogenation activity and 100% selectivity to *p*-CAN, owing to the electroconductivity of NC overcoating and the complete blockage of surface Pt sites from catalytic dechlorination. The cleavage of C–Cl bond was also suppressed on Pt/Al_2O_3@NC-25 after calcination treatment due the electrostatic repulsion between Cl groups and negatively charged Pt sites resulting from Pt–N interactions. Consecutive cycle test showed that Pt/Al_2O_3@NC-25 displayed a good catalytic stability. Findings in this work reveal that surface coating of supported noble metal by N-doped carbon is a promising strategy for fabricating highly selective and stable catalysts for catalytic hydrogenation reduction of *p*-CNB.

Conflicts of interest

There are no conflicts to declare.

Acknowledgements

The financial support from the National Natural Science Foundation of China (no. 21976086) is gratefully acknowledged.

Notes and references

1 A. M. Tafesh and J. Weiguny, *Chem. Rev.*, 1996, **96**, 2035–2052.
2 X. D. Wang, M. H. Liang, J. L. Zhang and Y. Wang, *Curr. Org. Chem.*, 2007, **11**, 299–314.
3 M. Pietrowski, *Curr. Org. Synth.*, 2012, **9**, 470–487.
4 A. Burawoy and J. P. Critchley, *Tetrahedron*, 1959, **5**, 340–351.
5 M. H. Liu, W. Y. Yu and H. F. Liu, *J. Mol. Catal. A: Chem.*, 1999, **138**, 295–303.
6 A. B. Dongil, L. Pastor-Perez, J. L. G. Fierro, N. Escalona and A. Sepulveda-Escribano, *Appl. Catal., A*, 2016, **513**, 89–97.
7 Q. Wei, Y. S. Shi, K. Q. Sun and B. Q. Xu, *Chem. Commun.*, 2016, **52**, 3026–3029.
8 B. Coq and F. Figueras, *Coord. Chem. Rev.*, 1998, **178**, 1753–1783.
9 H. Chen, D. P. He, Q. Q. He, P. Jiang, G. B. Zhou and W. S. Fu, *RSC Adv.*, 2017, **7**, 29143–29148.
10 X. Li, Y. Wang, L. Q. Li, W. Q. Huang, Z. C. Xiao, P. F. Wu, W. B. Zhao, W. Guo, P. Jiang and M. H. Liang, *J. Mater. Chem. A*, 2017, **5**, 11294–11300.
11 N. Mahata, O. S. G. P. Soares, I. Rodriguez-Ramos, M. F. R. Pereira, J. J. M. Orfao and J. L. Figueiredo, *Appl. Catal., A*, 2013, **464**, 28–34.
12 M. H. Li, J. He, Y. Q. Tang, J. Y. Sun, H. Y. Fu, Y. Q. Wan, X. L. Qu, Z. Y. Xu and S. R. Zheng, *Chemosphere*, 2019, **217**, 742–753.
13 D. P. He, X. D. Jiao, P. Jiang, J. Wang and B. Q. Xu, *Green Chem.*, 2012, **14**, 111–116.
14 G. X. Chen, C. F. Xu, X. Q. Huang, J. Y. Ye, L. Gu, G. Li, Z. C. Tang, B. H. Wu, H. Y. Yang, Z. P. Zhao, Z. Y. Zhou, G. Fu and N. F. Zheng, *Nat. Mater.*, 2016, **15**, 564–569.
15 A. Jalal and A. Uzun, *J. Catal.*, 2017, **350**, 86–96.
16 C. S. Lu, H. K. Ji, Q. W. Zhu, X. J. Zhang, H. Wang, Y. B. Zhou, Q. Q. Liu, J. J. Nie, J. T. Ying and X. N. Li, *J. Mater. Sci.*, 2019, **54**, 10153–10167.
17 H. Liu, K. Tao, C. Xiong and S. Zhou, *Catal. Sci. Technol.*, 2015, **5**, 405–414.
18 D. Zhu, L. Long, J. Sun, H. Wan and S. Zheng, *Appl. Surf. Sci.*, 2020, **504**, 144329.
19 F. Q. Leng, I. C. Gerber, P. Lecante, S. Moldovan, M. Girleanu, M. R. Axet and P. Serp, *ACS Catal.*, 2016, **6**, 6018–6024.
20 T. Fu, M. Wang, W. M. Cai, Y. M. Cui, F. Gao, L. M. Peng, W. Chen and W. P. Ding, *ACS Catal.*, 2014, **4**, 2536–2543.
21 M. H. Li, Y. Hu, H. Y. Fu, X. L. Qu, Z. Y. Xu and S. R. Zheng, *Chem. Commun.*, 2019, **55**, 11786–11789.
22 T. Wang, Z. Dong, T. Fu, Y. C. Zhao, T. Wang, Y. Z. Wang, Y. Chen, B. H. Han and W. P. Ding, *Chem. Commun.*, 2015, **51**, 17712–17715.
23 Y. Y. Chu, J. Cao, Z. Dai and X. Y. Tan, *J. Mater. Chem. A*, 2014, **2**, 4038–4044.
24 R. Arrigo, M. E. Schuster, Z. Xie, Y. Yi, G. Wowsnick, L. L. Sun, K. E. Hermann, M. Friedrich, P. Kast, M. Hävecker, A. Knop-Gericke and R. Schlögl, *ACS Catal.*, 2015, **5**, 2740–2753.

25 R. F. Nie, H. Z. Jiang, X. H. Lu, D. Zhou and Q. H. Xia, *Catal. Sci. Technol.*, 2016, **6**, 1913–1920.
26 Y. B. Li, C. B. Zhang, J. Z. Ma, M. Chen, H. Deng and H. He, *Appl. Catal., B*, 2017, **217**, 560–569.
27 H. L. Peng, Z. Y. Mo, S. J. Liao, H. G. Liang, L. J. Yang, F. Luo, H. Y. Song, Y. L. Zhong and B. Q. Zhang, *Sci. Rep.*, 2013, **3**, 1765.
28 T. Paryjczak and J. A. Szymura, *Z. Anorg. Allg. Chem.*, 1979, **449**, 105–114.
29 C. Amorim and M. A. Keane, *J. Colloid Interface Sci.*, 2008, **322**, 196–208.
30 K. F. Ortega, R. Arrigo, B. Frank, R. Schlogl and A. Trunschke, *Chem. Mater.*, 2016, **28**, 6826–6839.
31 Y. X. Han, J. Zhou, W. J. Wang, H. Q. Wan, Z. Y. Xu, S. R. Zheng and D. Q. Zhu, *Appl. Catal., B*, 2012, **125**, 172–179.
32 J. Z. Shyu and K. Otto, *Appl. Surf. Sci.*, 1988, **32**, 246–252.
33 J. C. Serrano-Ruiz, G. W. Huber, M. A. Sanchez-Castillo, J. A. Dumesic, F. Rodriguez-Reinoso and A. Sepulveda-Escribano, *J. Catal.*, 2006, **241**, 378–388.
34 X. M. Ning, H. Yu, F. Peng and H. J. Wang, *J. Catal.*, 2015, **325**, 136–144.
35 W. Shi, B. S. Zhang, Y. M. Lin, Q. Wang, Q. Zhang and D. S. Su, *ACS Catal.*, 2016, **6**, 7844–7854.
36 J. P. Macquet, M. M. Millard and T. Theophanides, *J. Am. Chem. Soc.*, 1978, **100**, 4741–4746.
37 H. N. Pham, A. E. Anderson, R. L. Johnson, T. J. Schwartz, B. J. O'Neill, P. Duan, K. Schmidt-Rohr, J. A. Dumesic and A. K. Datye, *ACS Catal.*, 2015, **5**, 4546–4555.
38 B. Sun, T. J. Fu and H. C. Zeng, *Chem. Commun.*, 2018, **54**, 7030–7033.
39 Q. Xu, X. M. Liu, J. R. Chen, R. X. Li and X. J. Li, *J. Mol. Catal. A: Chem.*, 2006, **260**, 299–305.
40 S. Iihama, S. Furukawa and T. Komatsu, *ACS Catal.*, 2016, **6**, 742–746.
41 Y. Sheng, X. G. Wang, Z. K. Xing, X. B. Chen, X. J. Zou and X. G. Lu, *ACS Sustainable Chem. Eng.*, 2019, **7**, 8908–8916.
42 M. R. Gray, Y. Zhao and C. M. McKnight, *Fuel*, 2000, **79**, 285–294.
43 M. Zhou, M. Li, C. Hou, Z. Li, Y. Wang, K. Xiang and X. Guo, *Chin. Chem. Lett.*, 2018, **29**, 787–790.